

# Alpha-resonance structure in $^{11}\text{C}$ studied via resonant scattering of $^7\text{Be}+\alpha$ and $^7\text{Be}(\alpha, p)$ reaction

H. Yamaguchi\* and D. Kahl

*Center for Nuclear Study, the University of Tokyo,  
RIKEN Campus, 2-1 Hirosawa, Wako, Saitama 351-0198, Japan*

Y. Wakabayashi and S. Kubono

*The Institute of Physical and Chemical Research (RIKEN),  
2-1 Hirosawa, Wako, Saitama 351-0198, Japan*

T. Hashimoto

*Research Center for Nuclear Physics, Osaka University,  
10-1 Mihogaoka, Ibaraki, Osaka 567-0047, Japan*

S. Hayakawa

*Laboratori Nazionali del Sud, Istituto Nazionale di Fisica Nucleare, Via S. Sofia 62, 95125 Catania, Italy*

T. Kawabata

*Department of Physics, Kyoto University, Kita-Shirakawa, Kyoto 606-8502, Japan*

N. Iwasa

*Department of Physics, Tohoku University, Aoba, Sendai, Miyagi 980-8578, Japan*

T. Teranishi

*Department of Physics, Kyushu University, 6-10-1 Hakozaki, Fukuoka 812-8581, Japan*

Y.K. Kwon

*Institute for Basic Science, 70, Yuseong-daero 1689-gil, Yuseong-gu, Daejeon 305-811, Korea*

D.N. Binh, L.H. Khiem, and N.N. Duy

*Institute of Physics, Vietnam Academy of Science and Technology,  
18 Hong Quoc Viet, Nghia do, HaNoi, Vietnam*

(Dated: December 27, 2012)

**Background:** The resonance structure in  $^{11}\text{C}$  is particularly of interest with regard to the astrophysical  $^7\text{Be}(\alpha, \gamma)$  reaction, relevant at high temperature, and to the  $\alpha$ -cluster structure in  $^{11}\text{C}$ .

**Purpose:** The measurement was to determine unknown resonance parameters for the high excited states of  $^{11}\text{C}$ . In particular, the  $\alpha$  decay width can be useful information to discuss  $\alpha$  cluster structure in  $^{11}\text{C}$ .

**Methods:** New measurements of the  $^7\text{Be}+\alpha$  resonant scattering and the  $^7\text{Be}(\alpha, p)^{10}\text{B}$  reaction in inverse kinematics were performed for center-of-mass energy up to 5.5 MeV, and the resonances at excitation energies of 8.9–12.7 MeV in the compound  $^{11}\text{C}$  nucleus were studied. Inelastic scattering of  $^7\text{Be}+\alpha$  and the  $^7\text{Be}(\alpha, p_1)^{10}\text{B}^*$  reaction were also studied with a simultaneous  $\gamma$ -ray measurement. The measurements were performed at the low-energy RI beam facility CRIB (CNS Radioactive Ion Beam separator) of the Center for Nuclear Study (CNS), the University of Tokyo.

**Results:** We obtained excitation functions of  $^7\text{Be}(\alpha, \alpha_0)^7\text{Be}$  (elastic scattering),  $^7\text{Be}(\alpha, \alpha_1)^7\text{Be}^*$  (inelastic scattering),  $^7\text{Be}(\alpha, p_0)^{10}\text{B}$ , and  $^7\text{Be}(\alpha, p_1)^{10}\text{B}^*$ . Many resonances including a new one were observed and their parameters were determined by an R-matrix analysis.

**Conclusions:** The resonances we observed possibly enhance the  $^7\text{Be}(\alpha, \gamma)$  reaction rate but in a smaller magnitude than the lower-lying resonances. A new negative-parity cluster band, similar to the one previously suggested in the mirror nucleus  $^{11}\text{B}$ , is proposed.

PACS numbers: 25.55.-e, 24.30.-v, 21.60.Gx

## I. INTRODUCTION

The  $^7\text{Be}(\alpha, \gamma)^{11}\text{C}$  reaction is considered to play an important role in the hot  $pp$  chain and related reaction

---

\* yamag@cns.s.u-tokyo.ac.jp

sequences [1]. Several reaction sequences including the  ${}^7\text{Be}(\alpha, \gamma){}^{11}\text{C}$  reaction should take place in some high-temperature environments. One of those sequences is called  $pp$ -V,

$${}^7\text{Be}(\alpha, \gamma){}^{11}\text{C}(\beta^+\nu){}^{11}\text{B}(p, 2\alpha){}^4\text{He}.$$

Others are rap (II, III and IV) sequences,

$${}^7\text{Be}(\alpha, \gamma){}^{11}\text{C}(p, \gamma){}^{12}\text{N}(p, \gamma){}^{13}\text{O}(\beta^+\nu){}^{13}\text{N}(p, \gamma){}^{14}\text{O},$$

$${}^7\text{Be}(\alpha, \gamma){}^{11}\text{C}(p, \gamma){}^{12}\text{N}(\beta^+\nu){}^{12}\text{C}(p, \gamma){}^{13}\text{N}(p, \gamma){}^{14}\text{O},$$

and

$${}^7\text{Be}(\alpha, \gamma){}^{11}\text{C}(\alpha, p){}^{14}\text{N}(p, \gamma){}^{15}\text{O},$$

which are reaction chains to synthesize CNO nuclei without the triple- $\alpha$  process, effective at  $T_9 > 0.2$ , where  $T_9$  is the temperature in GK. At  $T_9$  below 0.2,  ${}^7\text{Be}$  predominantly makes an electron capture, almost independent of the density. The  ${}^7\text{Be}(\alpha, \gamma){}^{11}\text{C}$  reaction and these sequences possibly play important roles in the explosion of supermassive objects with lower metallicity [2], novae [3] and big-bang nucleosynthesis [4, 5]. The  ${}^7\text{Be}(\alpha, \gamma){}^{11}\text{C}$  reaction rate is greatly affected by the resonances. At the lowest temperature, there is a large contribution to the reaction rate by the subthreshold resonance at the excitation energy  $E_{\text{ex}} = 7.50$  MeV. The two resonances located at  $E_{\text{ex}} = 8.11$  MeV and  $E_{\text{ex}} = 8.42$  MeV determine the rate at higher temperature around  $T_9 = 0.5$ – $1$ . Higher excited states may contribute to the reaction rates at  $T_9 > 1$ . A recent theoretical calculation [6] of the  $\nu p$ -process in core-collapse supernovae [7] shows that the  ${}^7\text{Be}(\alpha, \gamma)$  reaction may contribute as much as the triple- $\alpha$  process to the synthesis of elements heavier than boron at the relevant temperature of  $T_9 = 1.5$ – $3$ . Therefore, it is also important to study the resonances for such a high temperature region, corresponding to  $E_{\text{ex}} \sim 8$ – $10$  MeV in the Gamow energy window.

The information on the excited states in  ${}^{11}\text{C}$  is still limited. Resonance states above  $E_{\text{ex}} = 9$  MeV have been studied via  ${}^{10}\text{B}(p, \alpha)$  and other reactions such as  ${}^{12}\text{C}(p, d){}^{11}\text{C}$  [8–17]. The resonances typically have widths of the order of 100 keV, but their  $\alpha$ -decay widths  $\Gamma_\alpha$  are not known with a good precision, and even the spin and parity ( $J^\pi$ ) have not been clearly determined yet for some of the states. The excited states at lower energies ( $E_{\text{ex}} = 8$ – $9$  MeV) have narrower particle widths, and  $\Gamma_\alpha$  are only known for two resonances located at  $E_{\text{ex}} = 8.11$  and  $8.42$  MeV. The  ${}^7\text{Be}(\alpha, \gamma){}^{11}\text{C}$  reaction cross section was directly measured only at the energies of these two resonances [18].

Another interest for the  ${}^7\text{Be}+\alpha$  system is its nuclear cluster structure. The  $3/2_3^-$  state in  ${}^{11}\text{C}$  at  $E_{\text{ex}} = 8.11$  MeV is regarded as a dilute cluster state similar to the one in  ${}^{12}\text{C}$  [19], where two  $\alpha$  particles and  ${}^3\text{He}$  are weakly interacting and spatially extended. Its exotic structure is attracting much attention [20]. The cluster structure

in  ${}^{11}\text{B}$ , the mirror nucleus of  ${}^{11}\text{C}$ , was studied by measuring its isoscalar monopole and quadrupole strengths in the  ${}^{11}\text{B}(d, d')$  reaction [21, 22]. As a result, they indicated that the 8.56-MeV state in  ${}^{11}\text{B}$ , the mirror of the 8.11-MeV state in  ${}^{11}\text{C}$ , is considered to have a dilute cluster structure. Besides this state, rotational bands in  ${}^{11}\text{B}$  and  ${}^{11}\text{C}$ , which might be related to the  $\alpha$  cluster structure, have been discussed [23, 24]. In our recent study of  ${}^{11}\text{B}$  by  ${}^7\text{Li}+\alpha$  resonant elastic scattering, we observed strong  $\alpha$  resonances, and we determined their  $\Gamma_\alpha$ . A new cluster band with negative parity was also suggested in the highly excited states [25].

In the present study, we performed a measurement of the  ${}^7\text{Be}+\alpha$  resonant elastic scattering to study resonance structure of  ${}^{11}\text{C}$ , complementary to the previous study [25]. We also measured protons from  ${}^7\text{Be}(\alpha, p){}^{10}\text{B}$  reactions, which have been studied mostly by its inverse reaction. The actual measurements were performed in inverse kinematics,  ${}^4\text{He}({}^7\text{Be}, \alpha)$  and  ${}^4\text{He}({}^7\text{Be}, p)$ , but we denote these as  ${}^7\text{Be}(\alpha, \alpha)$  and  ${}^7\text{Be}(\alpha, p){}^{10}\text{B}$  for consistency. The strengths of the resonances in the present study should provide useful information on the  $\alpha$ -cluster structure of  ${}^{11}\text{C}$  and on the astrophysical  ${}^7\text{Be}(\alpha, \gamma)$  reaction rate. Recently, a similar measurement independently planned at other facilities was carried out and published by Freer *et al.* [26]. We will present our new results and discuss the differences of the two new measurements. An essential difference is that we have measured  $\gamma$ -rays to obtain excitation functions of  ${}^7\text{Be}(\alpha, \alpha_1){}^7\text{Be}^*$  and  ${}^7\text{Be}(\alpha, p_1){}^{10}\text{B}^*$  reactions, which was not considered in [26].

## II. METHOD

The measurement was performed at the low-energy RI beam facility CRIB [27, 28], using the thick target method in inverse kinematics [29] to obtain excitation functions of elastic scattering and others for  $E_{\text{ex}} = 8.7$ – $13.0$  MeV in  ${}^{11}\text{C}$ . The experimental setup is almost identical to the one used in our  ${}^7\text{Li}+\alpha$  measurement [25], except that the beam was an RI beam produced at CRIB. A pure and intense  ${}^7\text{Be}$  beam can be produced in-flight at CRIB using a cryogenic gas target [30]. In the present measurement, a  ${}^7\text{Be}$  beam was produced using a 2.3-mg/cm<sup>2</sup>-thick hydrogen gas target and a  ${}^7\text{Li}$  beam at 5.0 MeV/u accelerated with an AVF cyclotron. Having an 8.5- $\mu\text{m}$  Havar foil as an energy degrader after the beam-production target, a low-energy  ${}^7\text{Be}$  beam at 17.9 MeV was produced. The  ${}^7\text{Be}$  beam was separated and purified by magnetic analysis and velocity selection with a Wien filter. The purity of the  ${}^7\text{Be}$  beam was about 30% and almost 100% before and after the Wien filter, respectively. The experimental setup after the Wien filter is shown in Fig. 1. The beam collimator was a  $20 \times 20$ -mm<sup>2</sup> rectangular aperture, accepting a large fraction of the transported beam.

A Micro-Channel Plate (MCP) was used for the detection of the beam position and timing. A CsI-deposited

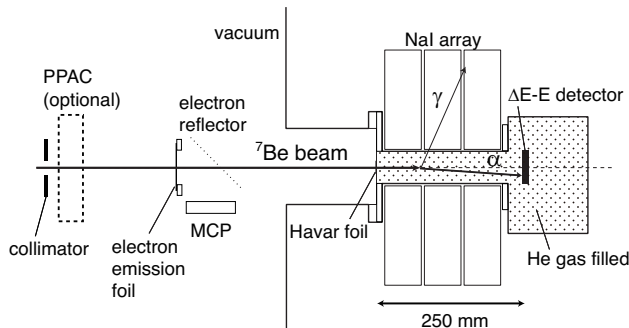


FIG. 1. Experimental setup of the measurement of the  ${}^7\text{Be} + \alpha$  elastic scattering and others in inverse kinematics.

0.7- $\mu\text{m}$ -thick aluminum foil was placed on the beam axis for the secondary electron emission. The secondary electrons were accelerated along the beam axis and reflected by  $90^\circ$  at a biased thin-wire reflector and detected at the MCP with a two-dimensional delay-line readout.

The gas target consisted of a 50-mm-diameter duct and a subsequent small chamber. Helium gas at 815 Torr was filled in the chamber and sealed with a 2.5- $\mu\text{m}$ -thick Havar foil as the beam entrance window. The  ${}^7\text{Be}$  beam energy after the entrance window of the helium gas target was measured as  $(15.43 \pm 0.13)$  MeV.  $\alpha$  particles recoiling to the forward angles were detected by the  $\Delta E$ - $E$  detector. The detector, consisting of 20- $\mu\text{m}$ - and 490- $\mu\text{m}$ -thick silicon detectors, was placed in the gas chamber. The helium gas was sufficiently thick to stop the  ${}^7\text{Be}$  beam in it before reaching the  $\Delta E$ - $E$  detector. The distance from the beam entrance window to the detector was 250 mm. Each detector had an active area of  $50 \times 50$  mm, and 16 strips for one side, making pixels of  $3 \times 3$  mm<sup>2</sup>. These detectors were calibrated with  $\alpha$  sources, as well as with proton and  $\alpha$  beams at various energies produced during the run. Each detector had an energy resolution better than 1.5% in full width at half maximum (FWHM) for 5-MeV  $\alpha$  particles. The measurement using the proton and  $\alpha$  beams was also for the evaluation of the dead-layer thickness between the two detectors. To measure 429-keV  $\gamma$  rays from inelastic scattering to the first excited state of  ${}^7\text{Be}$ , Ten NaI(Tl) detectors were placed around the duct and each NaI(Tl) crystal had a geometry of  $50 \times 50 \times 100$  mm<sup>3</sup>. They covered 20–60% of the total solid angle, depending on the reaction position in the long target. The energy-dependent photopeak efficiency of the NaI array was measured at various positions in the gas target, using standard radioactive sources of  ${}^{137}\text{Cs}$ ,  ${}^{22}\text{Na}$  and  ${}^{60}\text{Co}$ . The efficiency was determined as 15–30% for 429-keV  $\gamma$  rays. The energy resolution was about 9% in FWHM against 662-keV  $\gamma$  rays.

Most of the particles measured at the  $\Delta E$ - $E$  detector were  $\alpha$  particles from the elastic scattering and protons from the  ${}^7\text{Be}(\alpha, p)$  reaction. Some are in coincidence with  $\gamma$  rays, as shown later. The typical  ${}^7\text{Be}$  beam intensity

used in the measurement was  $2 \times 10^5$  particles per second at the secondary target, and the main measurement using the helium-gas target was performed for 4 days, injecting  $2.9 \times 10^{10}$   ${}^7\text{Be}$  particles into the gas target. We performed another measurement using an argon-gas target of an equivalent thickness for 1 day to evaluate the background  $\alpha$  particles reaching to the the  $\Delta E$ - $E$  detector as a contamination in the secondary beam.

To obtain a correct cross section with the current thick-gas target method, one needs a correct reaction position which is determined by the geometrical information of the target and detector, and energy loss of the beam and  $\alpha$  particles. A measurement with a parallel-plate avalanche counter (PPAC) [31] in addition to the MCP was also performed for a short time to check if the cross section is consistent between two measurements with different reaction positions for the same  $E_{\text{cm}}$ . In that measurement, the  ${}^7\text{Be}$  beam energy after the entrance window was degraded to 12.2 MeV, due to the additional energy loss in the PPAC. As a result, the reaction position is shifted by 6 cm at maximum to the upstream direction, which also makes the solid angle smaller, as compared with the measurement with the MCP alone. We confirmed the cross sections finally obtained for both measurements were in a good agreement, showing that there is no large error in the determination of the reaction position.

### III. DEDUCTION OF EXCITATION FUNCTIONS

#### A. Particle identification

The particle identification performed with the  $\Delta E$ - $E$  detector for the helium and argon target measurements are shown separately as two-dimensional energy plots in Fig. 2, where the total energy deposition of particles is plotted against the energy deposition in the  $\Delta E$  counter. As illustrated,  $\alpha$  particles and protons were clearly separated. In the background run with argon gas, we observed non-negligible numbers of protons and  $\alpha$  particles as shown in Fig. 2 (b). They are considered as beam-like particles produced at the production target as contaminants in the  ${}^7\text{Be}$  beam, and reached the silicon detectors at the end of the beamline. Most of such particles should have been eliminated at the Wien filter, but a very small number comparable to the reaction products remained, possibly by scattering in the inner wall of the beamline or some other reason.

In Fig. 2 (a), one may notice the locus of the  $\alpha$  particles is branched at the total energy about 6 MeV. This branching is possibly attributed to the channeling effect [32, 33] of the thin silicon detector. In the background run, shown in Fig. 2 (b), only the left branch was prominent, which implies the background  $\alpha$  particles from upstream mainly comprise the left branch. We observed events in the background run also at the right branch, but the number was much smaller than the left branch. Such

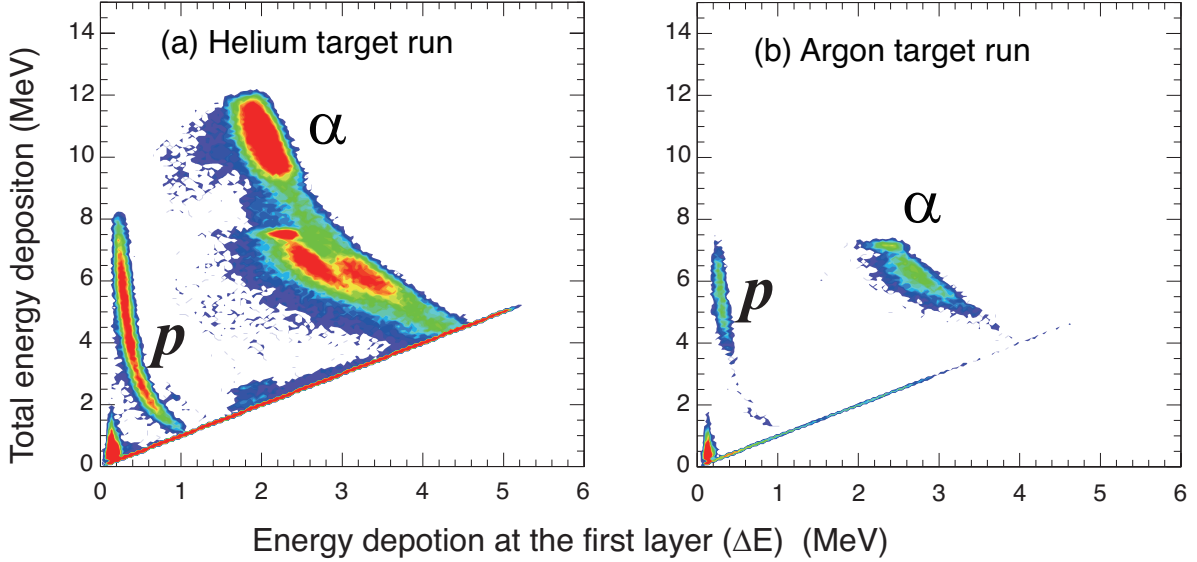


FIG. 2. (Color online)  $\Delta E$ - $E$  plot for the particle identification.

$\alpha$  particles had a strict limitation on the incoming angle which was almost perpendicular to the surface of the silicon detector and thus the channeling effect could be most prominent. On the other hand,  $\alpha$  particles from real scattering events had a broader range of angles and are less susceptible to the channeling effect. Although there was such a branching, we successfully evaluated the amount of background events by the argon-target measurement, to be subtracted from the data of the helium-target measurement. Performing the argon-target measurement was useful not only for the background evaluation, but also for understanding the unexpected origin of branching in the  $\alpha$  particles.

### B. Calculation of cross section

The energy of the  ${}^7\text{Be}$  beam at any position in the gas target was obtained with a good center-of-mass energy  $E_{\text{cm}}$  resolution (70 keV or better), based on a direct energy measurement at 7 different target pressures, compared with an energy loss calculation using the SRIM [34] code. Using this energy loss function, the energy of recoiled  $\alpha$  particle measured by the  $\Delta E$ - $E$  detector was converted to  $E_{\text{cm}}$ , calculating kinematical relationship for the elastic scattering. We selected events with an  $\alpha$  particle in coincidence with a  ${}^7\text{Be}$  beam particle measured in a  $20 \times 20 \text{ mm}^2$  square at the center of the MCP. The scattering angle determined from the detection position of the  $\Delta E$ - $E$  detector was used in the kinematical calculation as a correction. The energy loss of the recoiled  $\alpha$  particle in the gas target was calculated by SRIM and also considered in the calculation. The

differential cross section  $d\sigma/d\Omega$  was calculated for each small energy division using the solid angle of the detector, number of beam particles, and the effective target thickness. The solid angle was calculated by the geometrical information of the detector and the reaction position in the target determined by the kinematical calculation. The number of beam particles was obtained based on the single counting of the beam particle by the MCP, simultaneously recorded in the measurement. Note that it is very important to obtain a correct energy loss function in the target, since the target thickness and the solid angle, both directly reflected in the cross section, were also calculated using the function.

In a similar procedure but selecting proton events and using the kinematical relationship of the  ${}^7\text{Be}(\alpha, p){}^{10}\text{B}$  reaction, we obtained a spectrum containing  ${}^7\text{Be}(\alpha, p){}^{10}\text{B}$  reaction events.

Events of inelastic scattering  ${}^7\text{Be}(\alpha, \alpha_1){}^7\text{Be}^*$  producing  ${}^7\text{Be}^*$  at the first excited state were identified by measuring 429-keV  $\gamma$  rays with the NaI array. We selected triple-coincidence events in which a  ${}^7\text{Be}$  beam particle was detected at the beam detector (MCP), an  $\alpha$  or any other particle at the silicon detectors and a  $\gamma$ -ray at the NaI array. The  $\gamma$ -ray energy spectrum for those events is shown in Fig. 3. The peak at 429 keV was clearly identified, and small peaks around 511 keV and 718 keV, which should be from positron annihilations and excited  ${}^{10}\text{B}^*$  produced via the  ${}^7\text{Be}(\alpha, p_1){}^{10}\text{B}^*$  reaction respectively, were also observed. We performed a finer event discrimination by taking events in which an  $\alpha$  particle was identified and the beam is hitting at the central part of the MCP, an energy spectrum of  $\gamma$ -rays with a good signal-to-noise ratio was obtained, as shown in the insert of Fig. 3.

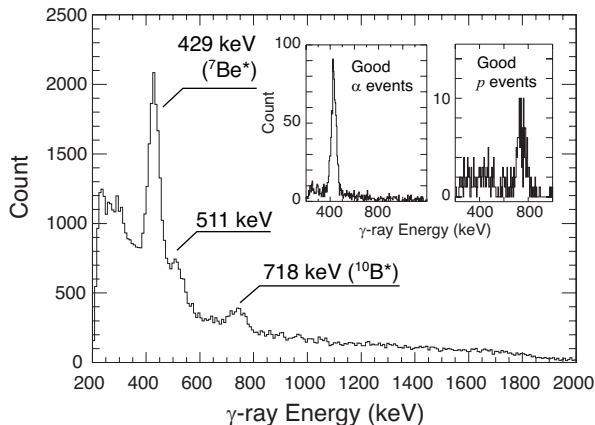


FIG. 3. Energy spectrum of  $\gamma$  rays for  ${}^7\text{Be}$ - $\alpha$ - $\gamma$  triple-coincidence events. The inserts show the same spectrum for events with an  $\alpha$  particle or  $p$  identified, after a beam position selection.

The events with a 429-keV  $\gamma$ -ray were used to obtain the excitation function of the inelastic scattering. A similar event discrimination was successfully performed for protons as also shown in the insert of the figure, to select events of the  ${}^7\text{Be}(\alpha, p_1){}^{10}\text{B}^*$  reaction. The photopeak efficiency of the NaI array, measured at various position in the gas target, was used for the calculation of the absolute cross section. Finally, excitation functions of the inelastic scattering and the  ${}^7\text{Be}(\alpha, p_1){}^{10}\text{B}^*$  reaction were obtained.

### C. Background Subtraction

The  ${}^7\text{Be}(\alpha, \alpha){}^7\text{Be}$  and  ${}^7\text{Be}(\alpha, p){}^{10}\text{B}$  spectra obtained by the above procedure still contain background  $\alpha$  and  $p$  contributions, the amount of which could be evaluated by the argon-target measurement. The background contribution to the differential cross sections were evaluated as shown in Fig. 4.

The sharp peak at 3.7 MeV in the background  $\alpha$  spectrum corresponds to  $\alpha$  particles which had the magnetic rigidity analyzed at the dipole magnets (D1 and D2) in CRIB. The broader lower-energy component is possibly from  $\alpha$  particles which had the same origin, but were scattered somewhere in the beamline. The heights of the sharp peak for both target runs are in good agreement, but the broad component was significantly higher in the helium-target spectrum. This suggests the peak around 3-3.5 MeV observed in the helium-target spectrum is partially due to the background  $\alpha$ , but the rest is by real scattering events. By subtracting the background contribution and the contribution of inelastic scattering events, we obtained an excitation function of elastic scattering.

There was no sharp peak in the background proton

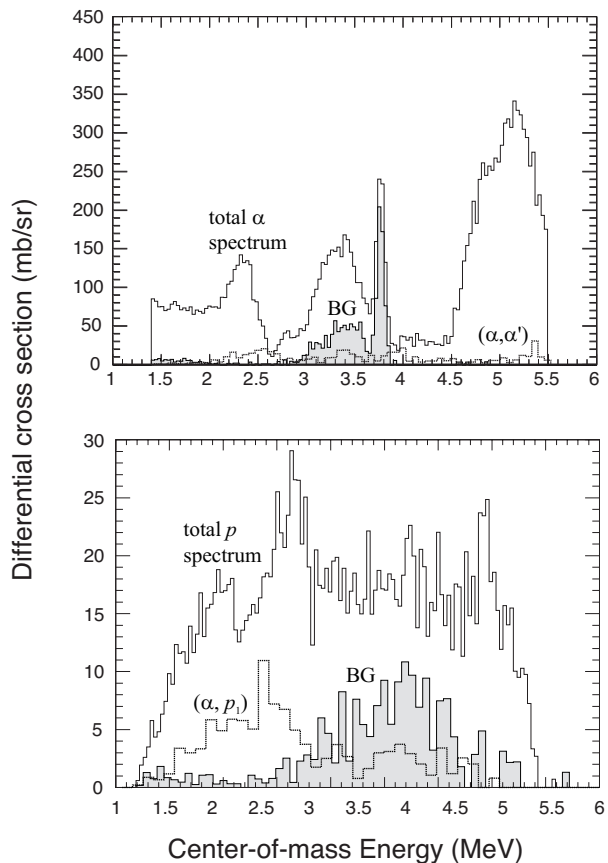


FIG. 4. Background subtraction for  $\alpha$  (upper) and  $p$  (lower) spectra. Total  $\alpha$  and  $p$  spectra are the excitation functions of  ${}^7\text{Be}(\alpha, \alpha){}^7\text{Be}$  and  ${}^7\text{Be}(\alpha, p){}^{10}\text{B}$ , but still containing background events. Shaded spectra show the contributions of background  $\alpha$  and  $p$  as beam contaminations. The spectra of  ${}^7\text{Be}(\alpha, \alpha_1){}^7\text{Be}^*$  and  ${}^7\text{Be}(\alpha, p_1){}^{10}\text{B}^*$  are also shown.

spectrum, but we performed a similar subtraction for the broad background and obtained the  ${}^7\text{Be}(\alpha, p){}^{10}\text{B}$  spectrum. The contribution from the  ${}^7\text{Be}(\alpha, p_1){}^{10}\text{B}^*$  reaction was also considered. Finally we obtained excitation functions for four different cross sections,  ${}^7\text{Be}(\alpha, \alpha_0){}^7\text{Be}$ ,  ${}^7\text{Be}(\alpha, \alpha_1){}^7\text{Be}^*$ ,  ${}^7\text{Be}(\alpha, p_0){}^{10}\text{B}$ , and  ${}^7\text{Be}(\alpha, p_1){}^{10}\text{B}^*$ . We refer to these excitation functions as the  $\alpha_0$ ,  $\alpha_1$ ,  $p_0$ , and  $p_1$  spectra, respectively, in the following sections. The excitation functions are shown in Fig. 5. The peak structure observed in the excitation functions should correspond to the resonances in  ${}^{11}\text{C}$ . The fitted curves are by an R-matrix analysis, which will be described later.

### D. Energy and angular uncertainty

Uncertainty in  $E_{\text{cm}}$  and averaged center-of-mass scattering angle  $\theta_{\text{cm}}$  are plotted for the  $\alpha_0$  and  $p_0$  spectra in Fig. 6, and the curves for  $\alpha_1$  and  $p_1$  spectra are quite similar to those.

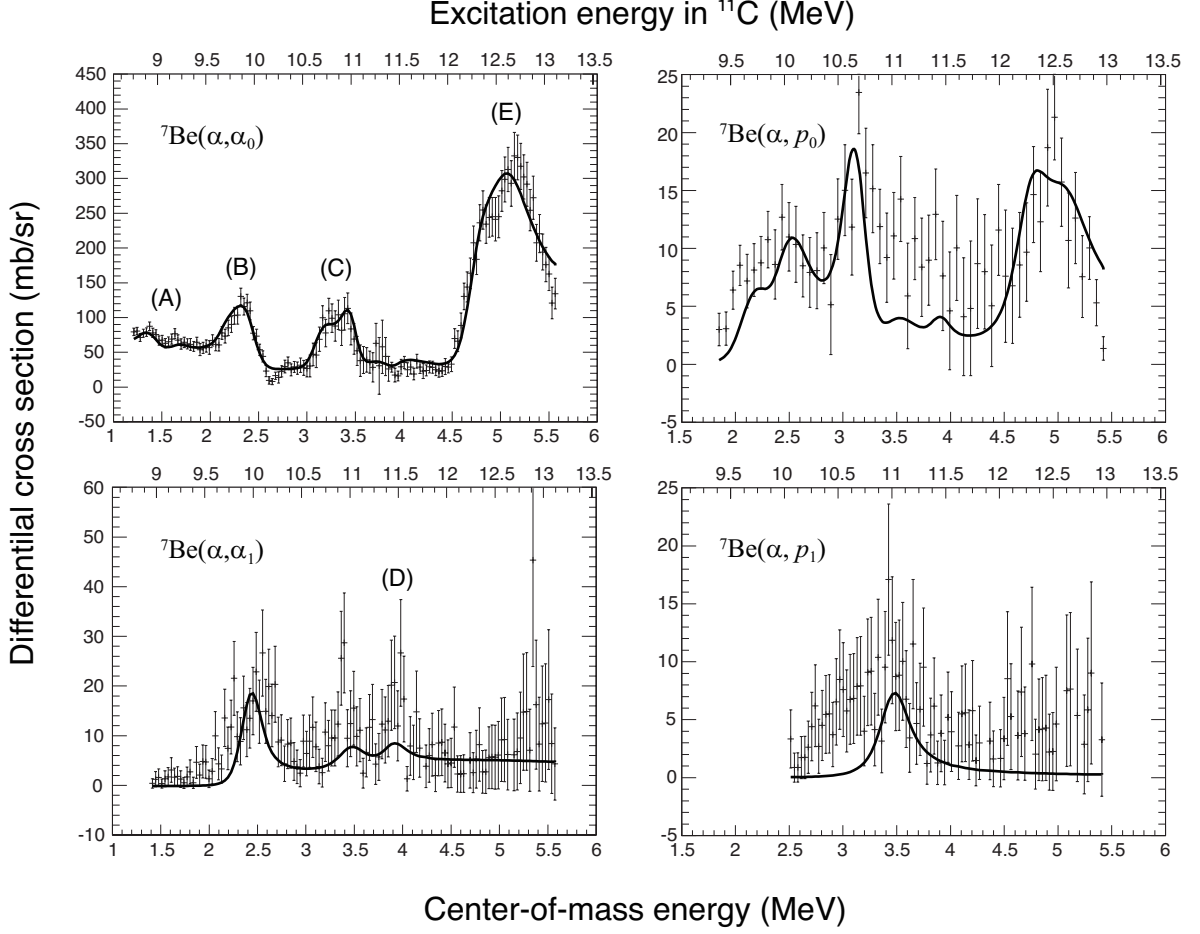


FIG. 5. Excitation functions, referred to as  $\alpha_0$ ,  $\alpha_1$ ,  $p_0$ , and  $p_1$  spectra. The best-fit curves by the R-matrix analysis are also shown. The labels (A–E) correspond to structures discussed in Sec. V.

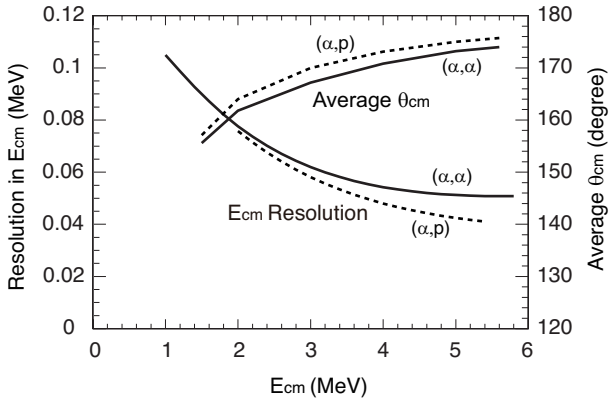


FIG. 6. Uncertainty in  $E_{\text{cm}}$  and averaged  $\theta_{\text{cm}}$  for the  $\alpha_0$  and  $p_0$  spectra.

For the  $\alpha_0$  spectrum, the overall uncertainty in  $E_{\text{cm}}$  was estimated as 70–130 keV, depending on the energy. The uncertainty mainly originated from the energy straggling of the  $^7\text{Be}$  beam and  $\alpha$  particles (30–80 keV), the energy resolution of the  $\Delta E$ - $E$  detector (20–55 keV), and the angular uncertainty due to the finite size of the detector (20–100 keV). The uncertainty is similar for the  $\alpha_1$  spectrum, and slightly better for the  $p_0$  and  $p_1$  spectra.

The excitation functions in Fig. 5 are for certain angular range covering  $\theta_{\text{cm}} = 180^\circ$ . The average  $\theta_{\text{cm}}$  was  $167^\circ$  at  $E_{\text{cm}} = 3$  MeV, but it depends on  $E_{\text{cm}}$ . The dependence is because the  $\Delta E$ - $E$  detector and the long helium gas target were closely arranged to obtain good statistics, and we had to select events within a fixed area of the detector in the analysis.

## IV. COMPARISON WITH PREVIOUS RESULTS

### A. Comparison with previous inverse reaction measurements

A direct comparison is possible for our  $p_0$  spectrum with the previous measurements of the inverse  $^{10}\text{B}(p, \alpha)^7\text{Be}$  reaction [11, 12, 15], although the measured scattering angles are not the same. The laboratory cross sections of the previous measurements were converted into the center-of-mass cross section, using the detailed balance theorem. The left panel in Fig. 7(a) shows the data in [12] with the laboratory angle  $\theta_{\text{lab}} = 150^\circ$  and the present measurement with an R-matrix calculation. The present measurement had a corresponding average angle in the inverse reaction of  $\theta_{\text{lab}} = 164^\circ$  (at  $E_{\text{cm}} = 3$  MeV). The right panel (b) shows the data in [11, 12, 15], all with  $\theta_{\text{lab}} = 90^\circ$ , but the present measurement data shown are the same as in (a). The curve for the present work is by an R-matrix calculation performed with the same resonant parameters as in (a), but with the angle adjusted to these previous measurements.

Considering the large uncertainty of our measurement, the overall features of the present spectrum are in agreement with previous measurements, such that the two peaks around 3 and 5 MeV are distinct. The absolute cross section shows a disagreement to some extent, but the previous measurements already had differences with one another as in Fig. 7(b). The cross section by [11] or [15] show a similar magnitude of the cross section with ours, but the angle is at  $\theta_{\text{lab}} = 90^\circ$ . The cross section by [12] at the same angle is lower than these two and our data at  $\theta_{\text{lab}} = 164^\circ$ . The angular dependence may partly explain the difference, as shown by the R-matrix curves at two different angles. One can see the calculation at  $\theta_{\text{lab}} = 90^\circ$  is closer to the data by [12] at  $\theta_{\text{lab}} = 90^\circ$ . The cross section of the present work at 3.5–4.5 MeV appears higher than any of previous data and the R-matrix calculation. We did not introduce strong resonances in this region to improve the fitting, since such resonances were not observed in the previous measurements. This discrepancy might be related to the background protons, which were distributed around 3–4.5 MeV, as shown in Fig. 4.

### B. Comparison with the latest inverse kinematics measurement

The measurement by Freer *et al.* [26] has been performed with essentially the same method as the present work. Here we compare the two results. The  $\alpha_0$  and  $p_0$  spectra of both measurements are compared in Fig. 8. The overall shapes of the two  $\alpha_0$  spectra have a common feature. There is a large double-peak structure around  $E_{\text{cm}} = 5$  MeV, and smaller peaks are located at an energy 1 MeV below, and at lower energies. However, two large differences are seen; the absolute cross section is different

by a factor 2–3 for the higher energy part, and the peaks are displaced in energy by about 500 keV. The cross section in [26] was normalized using the low-energy measurement data, and also by a Monte Carlo simulation, which may produce a systematic uncertainty as much as factor 2.5 at maximum, as they claim. On the other hand, our cross section is based on single counting of the beam particles and geometrical measurement. Furthermore, the previous  $^7\text{Li} + \alpha$  measurement [25] with the same analysis method yielded a consistent cross section with older normal kinematics measurements. Therefore, an error in the cross section by a factor 2–3 is unlikely to be produced in our measurement or analysis. In the thick target method, the energy can be easily shifted if the energy loss functions of the  $^7\text{Be}$  beam or the  $\alpha$  particle in the target is not correct. In our both measurements, the energy loss of the beam was directly measured over a wide range of pressures. We used the SRIM code for the energy loss of the  $\alpha$  particle, and the higher edge of  $E_{\text{cm}}$  from the measured data (5.5 MeV) was in good agreement with the  $E_{\text{cm}}$  expected from the measured beam energy at the beginning of the target. We do not expect an error in  $E_{\text{cm}}$  much more than 100 keV at  $E_{\text{cm}} \sim 5$  MeV. Another fact that may support the present work is that our spectrum could be explained with the known energy level information, as shown later, but in [26] it was necessary to introduce several new resonances to perform an R-matrix fit.

The  $p_0$  spectrum in [26] was separated into two energy regions. The lowest energy part perfectly agree with ours, but the data in [26] at higher energy again shows a lower cross section. However, the discrepancy is not obvious, since the deviation is comparable to the uncertainty, quite large in both measurements.

## V. R-MATRIX ANALYSIS

Several resonance structures were observed in our  $\alpha_0$  spectrum, namely, (A) Two small peaks at 8.9–9.2 MeV, (B) a peak around 10 MeV, (C) a broad peak at 10.5–11.0 MeV, considered to be a doublet, and (E) a doublet structure at 12–13 MeV, as shown in Fig. 5. Structures were also observed in the other three spectra, and some are corresponding to the peaks in the  $\alpha_0$  spectrum, and others are not, as (D) a small enhancement of the cross section in the  $\alpha_1$  spectrum at 11.4 MeV.

We performed an analysis using an R-matrix calculation code (SAMMY8 [35]) to deduce resonance parameters. The decay widths of four channels,  $\Gamma_{\alpha 0}$ ,  $\Gamma_{\alpha 1}$ ,  $\Gamma_{p 0}$ , and  $\Gamma_{p 1}$ , were considered in the R-matrix analysis. The basic strategy was as follows. First  $\Gamma_{\alpha 0}$  were roughly determined by an R-matrix fit of the  $\alpha_0$  spectrum, reproducing the peak structure. Using the  $\Gamma_{\alpha 0}$ , we analyzed the  $p_0$  spectrum and found the best values for  $\Gamma_{\alpha 0}$  and  $\Gamma_{p 0}$ . Then, the  $\alpha_0$  spectrum was analyzed again to determine  $\Gamma_{\alpha 0}$  more precisely. When  $\Gamma_{\alpha 0}$  and  $\Gamma_{p 0}$  were determined consistently by the two spectra, analysis was



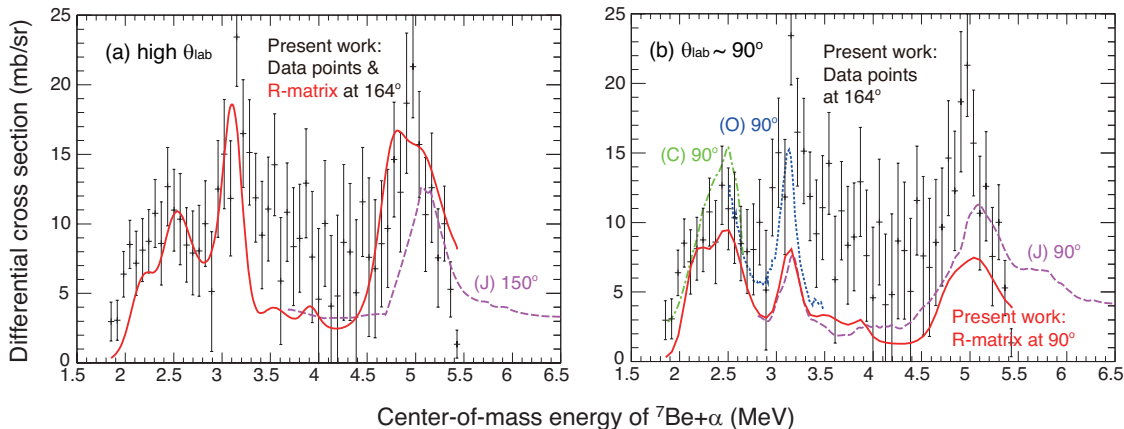


FIG. 7. (Color online) The  $p_0$  spectrum compared with previous measurements of the inverse  $^{10}\text{B}(p, \alpha)^7\text{Be}$  reaction by (J) Jenkin *et al.* [12], (C) Cronin *et al.* [11], and (O) Overley *et al.* [15]. R-matrix calculations performed at  $\theta_{\text{lab}} = 90^\circ$  and  $164^\circ$  are also shown. Note that the angles are in laboratory system of the  $^{10}\text{B}(p, \alpha)^7\text{Be}$  reaction.

performed for the  $\alpha_1$  and  $p_1$  spectra, both of which had low statistics and do not exhibit much structure. By repeating the above process until it converges, all the four widths,  $\Gamma_{\alpha 0}$ ,  $\Gamma_{\alpha 1}$ ,  $\Gamma_{p 0}$ , and  $\Gamma_{p 1}$ , were determined. To cope with many parameters in the fitting, we adopted resonant parameters by previous measurements [36] as much as possible. The detailed discussions for each structure we observed (A–E), including the  $J^\pi$  determination, are below. Another restriction we considered was that the sum of the decay widths do not exceed the known total width  $\Gamma_{\text{tot}}$  too much. The calculation was performed with channel radii  $R_c = 4.2$  fm for the  $^7\text{Be}+\alpha$  channel, and  $R_c = 3.8$  fm for the  $^{10}\text{B}+p$  channel. These channel radii were deviated by 20% for the evaluation of the uncertainties. The angle was fixed at  $\theta_{\text{cm}} = 167^\circ$  for the  $\alpha_0$  and  $\alpha_1$  spectra, and  $\theta_{\text{cm}} = 169^\circ$  for the  $p_0$  and  $p_1$ .

The results are summarized in Table I. The Wigner limit  $\Gamma_w = 2\hbar^2/\mu R^2 P_l$ , where  $\mu$  is the reduced mass and  $P_l$  is the penetrability, was calculated for an  $\alpha$  particle with an interaction radius  $R = 4.2$  fm and shown in the table for comparison. Uncertainties could be reasonably evaluated only for some  $\Gamma_{\alpha 0}$ , as shown in Table I, and the other widths could have very large uncertainties.

#### A. Peaks at 8.9–9.2 MeV

In this energy region the excitation function was rather flat in the  $\alpha_0$  spectrum, but two small bumps were observed. One of these may correspond to the known  $5/2^+$  state at 9.20 MeV [37]. The other one is located around 8.90 MeV. A resonance at this energy is not known by previous measurements and we regard this as a new resonance. However, it can be the same resonance as the one at 8.655 ( $7/2^+$ ) or 8.699 MeV ( $5/2^+$ ) [38], because the energy uncertainty in this lowest energy region is quite

large.

The 9.20-MeV resonance was initially introduced by Wiescher *et al.* [37] in their analysis of the  $^{10}\text{B}(p, \gamma)$  reaction measurement. Although a large total width of  $\Gamma_{\text{tot}} = 500$  keV was incorporated in the analysis of Ref. [37], our calculation with a large  $\Gamma_{p 0}$  resulted in diminishing the peak height, and a large  $\Gamma_{\alpha 0}$  far exceeding the Wigner limit becomes necessary. In the best fit,  $\Gamma_{p 0}$  was assumed to be 0.

For the 8.90-MeV bump, a resonance with  $l_\alpha = 3$  gives a good fit, and  $J^\pi = 9/2^+$  was the best among them. Other possible  $J^\pi$  were  $3/2^+$ ,  $5/2^+$ , and  $7/2^+$ . The resonance in this energy region may enhance the astrophysical  $^7\text{Be}(\alpha, \gamma)$  reaction rate, as shown later. However, it is difficult to derive conclusive resonance parameters with such small peaks broadened by the energy resolution, averaged for a broad range of angles. The current R-matrix calculation could be deceptive at the edge of our energy range. Therefore, it is desirable to perform another study for the resonances in this energy region.

#### B. Peak around 10 MeV

The  $\alpha_0$  spectrum exhibits a peak, which could be well reproduced by a resonance around 10.0 MeV having a large  $\Gamma_{\alpha 0}$ .

Four resonances at 9.65, 9.78, 9.97 and 10.083 MeV are known in this region [36]. The 9.78-MeV and 10.083-MeV resonances have been observed by many experiments. The former was by the  $^{10}\text{B}(p, \gamma)$  [8, 39] and  $^{10}\text{B}(p, \alpha)$  reactions [8–14], and the latter was by the  $^{10}\text{B}(p, \alpha)$  [8–11, 14] and  $^{10}\text{B}(d, n)$  reactions [15]. However, the  $J^\pi$  was in controversy for the former state [9, 15], while firmly determined as  $7/2^+$  for the latter one.

The current  $J^\pi$  assignments in this region were mostly



TABLE I. Best-fit resonance parameters of  $^{11}\text{B}$  determined by the present work. The  $E_{\text{ex}}$  and  $J^\pi$  shown in italic letters were fixed to those in [36, 38], and the others are proposed in the present work. See text for other possible  $J^\pi$  assignments.

$E_{\text{ex}}$ (MeV)	$J^\pi$	$l_{\alpha 0}$	$\Gamma_{\alpha 0}$ (keV)	$\Gamma_{p 0}$ (keV)	$\Gamma_{\alpha 1}$ (keV)	$\Gamma_{p 1}$ (keV)	$\Gamma_{\text{tot}}$ [38] (keV)	$\Gamma_{W_\alpha}$ (keV)
8.90	(9/2 <sup>+</sup> )	3	8					6.4
<i>9.20</i>	<i>5/2<sup>+</sup></i>	3	13				500	21
<i>9.65</i>	<i>(3/2<sup>-</sup>)</i>	0	20	50			210	1310
<i>9.78</i>	<i>(5/2<sup>-</sup>)</i>	2	19	100			240	450
<i>9.97</i>	<i>(7/2<sup>-</sup>)</i>	2	153±55	35	30		120	580
<i>10.083</i>	<i>7/2<sup>+</sup></i>	3	25	230			230	90
<i>10.679</i>	<i>9/2<sup>+</sup></i>	3	58±36	110			200	230
<i>11.03</i>	<i>(5/2<sup>-</sup>)</i>	3	130±83	25	45	120	300	360
<i>11.44</i>	<i>(3/2<sup>+</sup>)</i>	1	80	30	150		360	2680
<i>12.40</i>	<i>9/2<sup>+</sup></i>	3	460±150	90			1000–2000	1100
<i>12.65</i>	<i>(7/2<sup>+</sup>)</i>	3	420±178	110			360	1270

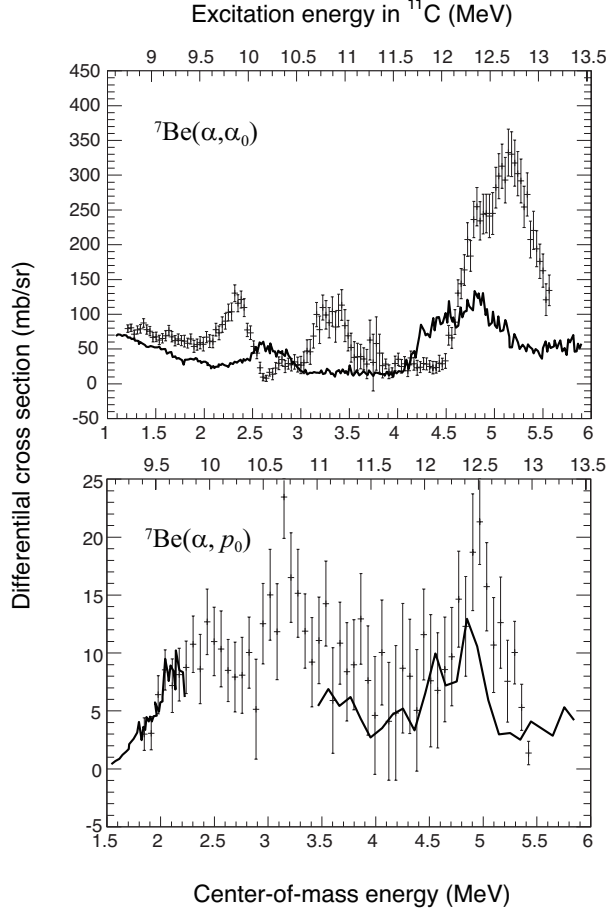


FIG. 8. The  $\alpha_0$  and  $p_0$  spectra by the present work and [26] (solid lines).

by Wiescher *et al.* [37]. They made tentative assignments of  $J^\pi$  for the three states at 9.65, 9.78 and 9.97 MeV as  $3/2^-$ ,  $5/2^-$ , and  $7/2^-$ , respectively, by an analysis of the  $^{10}\text{B}(p, \gamma)$  reaction measurement data. The 9.65 and 9.97 MeV states, which had not been known before, were introduced to reproduce their excitation functions. Later, a resonance near 9.97 MeV was also observed by the  $^{12}\text{C}(p, d)$  reaction [40], but  $J^\pi$  was not determined. No other observation of the 9.65-MeV resonance is known. The 9.65-MeV ( $3/2^-$ ), 9.78-MeV ( $5/2^-$ ), and 10.083-MeV ( $7/2^+$ ) states have candidates of their mirrors at 10.26, 10.34, 10.60 MeV in  $^{11}\text{B}$ , while the 9.97-MeV state has none.

We fully adopted the tentative  $J^\pi$  assignments in [37]. The absence of this resonance in the present  $p_0$  spectrum and previous  $^{10}\text{B}(\alpha, p)$  measurements suggests this 9.97-MeV resonance should have a much smaller  $\Gamma_{p 0}$  than the neighboring 9.78-MeV and 10.083-MeV resonances. There is a peak around 9.97 MeV also in the  $\alpha_1$  spectrum, and we introduced  $\Gamma_{\alpha 1}$  in the calculation to reproduce the peak.

### C. Doublet at 10.5–11.0 MeV

A peak was observed in the  $p_0$  spectrum, as previously observed by the inverse reaction [11, 12, 15]. There is a peak in the  $\alpha_0$  spectrum at the same  $E_{\text{cm}}$ , and the spectral shape suggests that it may be forming a doublet with another resonance at 11.0 MeV. For the higher component in the doublet, a good fit was obtained by a  $l_\alpha = 2$  resonance with  $J^\pi = 5/2^-$  or  $7/2^-$ .

A resonance at 11.03 MeV had been observed by  $^{11}\text{B}(^3\text{He}, t)$  [41],  $^{13}\text{C}(p, t)$  [42], and others [38]. However,  $J^\pi$  has not been determined, and only assumed as a state with an isospin  $T = 1/2$ .

In the  $p_1$  spectrum, a resonance was observed around 11.03 MeV as the only peak structure in the spectrum. This resonant shape could be reproduced by introducing a resonance with  $J^\pi = (3/2^-, 5/2^-, 7/2^-)$ , but the peak

height was significantly lower, when  $J^\pi$  was assumed to be  $3/2^-$ . There is a small peak-like structure also in the  $\alpha_1$  spectrum. The peak is consistent with a calculation introducing a  $J^\pi = 5/2^-$  resonance, although the agreement in the peak height is not obvious due to the large uncertainty. In a calculation with  $J^\pi = 7/2^-$ ,  $l_{\alpha 1} = 4$  was required for the  ${}^7\text{Be} + \alpha_1$  channel, and a good fit was not obtained. Here we adopt  $J^\pi = 5/2^-$  as the best assignment, but  $J^\pi = 7/2^-$  might be also possible, if we ignore the  $\alpha_1$  spectrum which has quite low statistics.

#### D. Structure at 11.4 MeV

A small enhancement of the cross section was identified at 11.4 MeV in the  $\alpha_1$  spectrum. A resonance at 11.44 MeV was observed by Jenkin *et al.* [12] by the  ${}^{10}\text{B}(p, \alpha_1){}^7\text{Be}^*$  reaction only at forward scattering angles, but the resonance was not clearly seen by the  ${}^{10}\text{B}(p, \alpha_0){}^7\text{Be}$  reaction. Their cross section of the  ${}^{10}\text{B}(p, \alpha_1){}^7\text{Be}^*$  reaction was simply decreasing as  $\theta_{\text{lab}}$  increases. The implication of this angular dependence was not discussed in detail. An R-matrix calculation with a single resonance cannot reproduce such an angular dependence asymmetric with regard to  $\theta_{\text{cm}} = 90^\circ$ . However, a resonance with a spin  $J=3/2-7/2$  can have a feature that the cross section decreases at backward angles toward  $\theta_{\text{cm}} = 180^\circ$ .

In the present  $p_0$  spectrum, we did not clearly observe the resonance either. This suggests the resonance should have a relatively large  $\Gamma_{\alpha 1}$ . Considering the absence of a sharp peak in the  $\alpha_0$  and  $p_0$  spectrum and the best R-matrix fitting for the  $\alpha_1$  spectrum, we tentatively assigned  $J^\pi$  as  $3/2^+$ , but  $J^\pi = 3/2^-$ ,  $5/2^\pm$ , and  $7/2^\pm$  might be possible. Note that this resonance in the  $\alpha_0$  spectrum is closely located to the sharp peak in the background contribution as shown in Fig. 4, and a small structure could be lost.

#### E. Doublet at 12–13 MeV

In this energy region, we observed a double-peak structure in the  $\alpha_0$  spectrum with a large cross section.

Ignoring isospin  $T = 3/2$  states, resonances at 12.4 and 12.65 MeV have been known previously. In a previous  ${}^{10}\text{B}(p, \alpha){}^7\text{Be}$  reaction measurement [12], a broad resonance having a large width of 400 keV was observed. Assuming a single level at 12.65 MeV, they tentatively determined  $J^\pi$  as  $7/2^+$ . The 12.4-MeV resonance was observed by the  ${}^{10}\text{B}(p, \gamma){}^7\text{Be}$  reaction [43], and by the  ${}^{12}\text{C}({}^3\text{He}, \alpha)$  reaction. In [43], the width was determined as 1–2 MeV and it was discussed as a part of a giant resonance.

In the present work, the observed double-peak structure was fitted by the  $7/2^+$  resonance at 12.65 MeV, and another resonance at 12.4 MeV. The best fit was made with  $J^\pi = 9/2^+$  for the 12.4-MeV resonance. The fit was

unsatisfactory by any other  $J^\pi$ , although it was considered as a negative parity state in [43]. Freer *et al.* [26] also explained this structure as a doublet consisting of  $9/2^+$  and  $7/2^+$  resonances, although the doublet is displaced in energy by several 100 keV, and the ordering is reversed. The broad peak we observed in the  $p_0$  spectrum at the same energy was also fitted by the doublet of the same two states.

## VI. DISCUSSION

### A. Alpha-cluster bands

The strong resonances we have observed in the  $\alpha_0$  spectrum have large  $\Gamma_{\alpha 0}$ , which are reflecting their property of  $\alpha$ -cluster structure. Fig. 9 shows resonant states in  ${}^{11}\text{B}$  and  ${}^{11}\text{C}$  observed in the present work and our previous work [25]. We can identify several pairs of mirror states, as indicated in the figure. The difference in  $E_{\text{ex}}$  is about 500 keV for the lower pairs of states and smaller for the highest two. Such energy difference between mirror states was discussed in [26] in relation with the phase transition from shell-model states to cluster states [44, 45].

Rotational bands in  ${}^{11}\text{B}$  and  ${}^{11}\text{C}$ , which might be related to the cluster structure, had been discussed in [23, 24]. In our previous work [25], we have indicated that the 12.63 MeV resonance in  ${}^{11}\text{B}$  may have  $J^\pi = 9/2^+$ , as initially mentioned in [24]. We also proposed a new negative-parity band, of which the head is the 8.56-MeV ( $J^\pi = 3/2^-$ ) state. According to a recent calculation based on antisymmetrized molecular dynamics (AMD) method [46], this can be interpreted as a negative-parity band having a large  $B(E2)$  of 20–30  $e^2\text{fm}^4$ , and the members should have a  $2\alpha$ - $t$  cluster structure. The energy of the band head appeared as lower than the line expected from the other members, in both the experiment and theory. In [46], the lowering in the level energy was attributed to the relatively weak interactions between  $2\alpha$ - $t$  in the 8.56-MeV state, making a deviation from the higher states which have a more rigid structure.

A similar discussion can be applied to  ${}^{11}\text{C}$ . Two positive-parity rotational bands,  $K = 3/2^+$  and  $5/2^+$ , were suggested in [24]. We observed a strong resonance with  $J^\pi = 9/2^+$  at 12.4 MeV in  ${}^{11}\text{C}$ , and it can be the missing member of the  $K = 3/2^+$  rotational band. We propose a new negative-parity band also in  ${}^{11}\text{C}$ , as shown in Fig. 10. The members of the band could have a  $2\alpha$ - ${}^3\text{He}$  cluster structure. The head is the 8.10-MeV ( $J^\pi = 3/2^-$ ) state, the mirror of the 8.56-MeV state in  ${}^{11}\text{B}$ . The second member is the 9.78-MeV state, assigned as  $J^\pi = 5/2^-$  previously. The third member can be the state at 11.03 MeV. Our assignment was either  $J^\pi = 5/2^-$  or  $7/2^-$ , and the latter assignment agrees with the systematics of this negative band. The systematics predicts there can be a  $J^\pi = 9/2^-$  state around 13 MeV. A candidate is the 12.65-MeV state. In the present

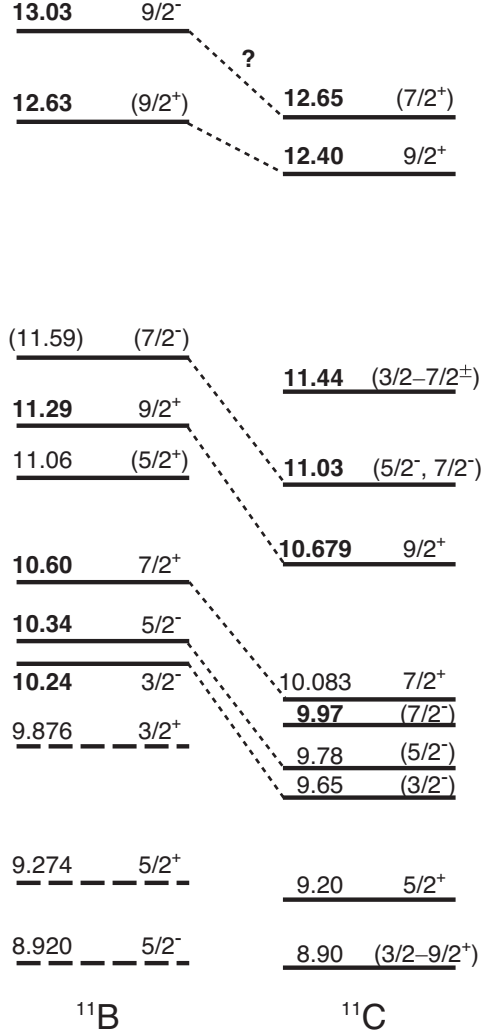


FIG. 9. Resonant states observed in the present work and our previous work [25].  $E_{\text{ex}}$  in MeV and  $J^\pi$  in our works are shown for each state, and the states with an  $E_{\text{ex}}$  in bold letters were observed as significant resonant peaks. The states with dashed lines were not observed in our measurements, but taken from [38].

work, this state was regarded to form a doublet together with the 12.4-MeV state. A similar doublet was observed in the mirror nucleus [25], and the higher state was considered to have  $J^\pi = 9/2^-$  (see Fig. 9). If the tentative assignment of  $J^\pi = 7/2^+$  was wrong, the 12.65-MeV state may have  $J^\pi = 9/2^-$ , as in the mirror nucleus. Another candidate is the resonance at 13.4 MeV [38], which is known to have a certain  $\alpha$  width, but its  $J^\pi$  has not been determined. In Fig. 10, these states are shown as circles and connected as dotted lines under the assumption that they have  $J^\pi = 9/2^-$ . The energy of the band head (8.10 MeV) appears as lower than the systematics expected from the higher state. This lowering is in agreement with the mirror state [25, 46].

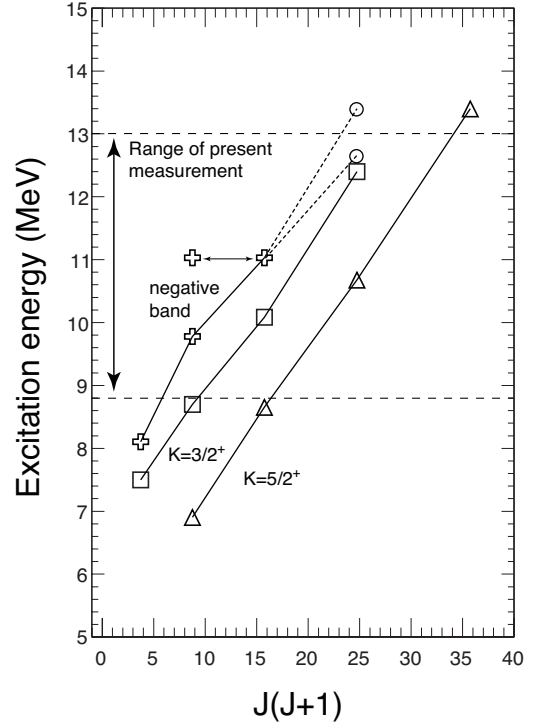


FIG. 10. Two positive-parity rotational bands in  $^{11}\text{C}$  suggested in [24], and a newly proposed negative-parity band.

A problem is that the  $\Gamma_{\alpha 0}$  of the 9.78-MeV ( $5/2^-$ ) resonance is not large, while the neighboring 9.97-MeV resonance with  $J^\pi = 7/2^-$  has a larger  $\Gamma_{\alpha 0}$ , being more likely to be an  $\alpha$ -cluster state. The previous studies in the mirror nucleus [25, 38] show there is no such corresponding state with  $J^\pi = 7/2^-$  in  $^{11}\text{B}$ , as shown in Fig. 9. In this respect, the current identification of the resonances and the  $J^\pi$  assignments for  $E_{\text{ex}} = 9.5$ –10 MeV can be questioned.

## B. Astrophysical reaction rate of $^7\text{Be}(\alpha, \gamma)$

The resonances observed in the present work might contribute to the astrophysical  $^7\text{Be}(\alpha, \gamma)^{11}\text{C}$  reaction rate at high temperature,  $T_9 > 1.5$ . Here we calculate the resonant reaction rate and compare it with the total reaction rate evaluated in NACRE [47, 48]. In the evaluation in NACRE, only 2 resonances at 8.1045 and 8.420 MeV are included. These two resonances dominate the reaction rate  $N_A \langle \sigma v \rangle$  up to the temperature  $T_9 \sim 3$ , and a Hauser-Feshbach calculation rate was included for the higher temperature.

The resonant reaction rates were calculated for three resonances using analytical formula described in [47], and plotted in Fig. 11. The total reaction rate evaluated by NACRE and its recently updated rate (NACRE-II) [48] are also shown for comparison. Table II shows the pa-

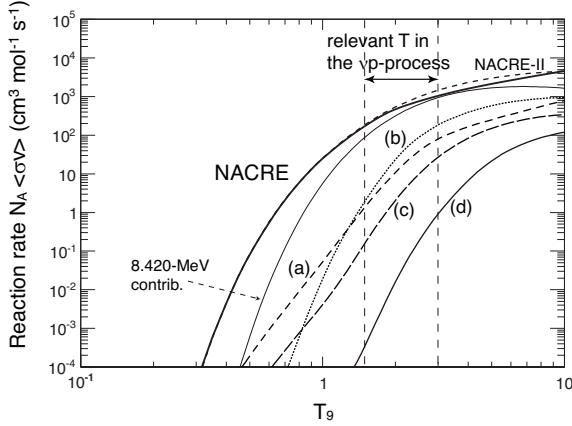


FIG. 11. Resonant reaction rate of  ${}^7\text{Be}(\alpha, \gamma)$  for the 8.90, 9.20, and 9.97-MeV resonances, calculated by the analytical formula (see text and Table II for the labels). The evaluation by NACRE and NACRE-II are shown for comparison. The contribution by the 8.420-MeV resonance, included in NACRE, is also shown.

rameters we used in the calculation. The  $\Gamma_\gamma$  and the decay scheme are experimentally unknown for this energy range. Therefore, we evaluated  $\Gamma_\gamma$  by a calculation based on the Weisskopf unit with a spectroscopic factor of 0.1, which roughly reproduces the experimentally known  $\Gamma_\gamma$  of the 8.1045 and 8.420-MeV resonances. Note that such a spectroscopic factor was not explicitly used in the plot of our previous publication [25]. The labels (a)–(d) in Fig. 11 correspond to the ones in Table II. (a) is for our newly identified resonance at 8.90 MeV.  $J^\pi$  was taken to be  $9/2^+$  from our best fit. Since the  $J^\pi$  assignment may not be correct, we also evaluated the contribution for the same resonance, but when the resonance had a lower spin of  $3/2$ , shown as (b). Basically (b) contributes to the reaction rate more, but its tail contribution is smaller than (a). For  $T_9 = 2$ – $3$ , where the 8.420-MeV resonance dominates the reaction rate, the contribution of the 8.90-MeV was evaluated as around 10% of the total reaction rate. (c) is for the 9.20-MeV resonance, where we also found a small peak in the  $\alpha_0$  spectrum. We used  $J^\pi = 5/2^+$  and  $\Gamma_{\text{tot}} = 500$  keV from previous measurements, although such a large  $\Gamma_{\text{tot}}$  was inconsistent with our R-matrix analysis. (d) is for the 9.97-MeV resonance, which was identified as a strong alpha resonance in the  $\alpha_0$  spectrum. The tentative assignment of  $J^\pi = 7/2^-$  [37] was used for the evaluation, and a smaller contribution was obtained, as shown in Fig. 11. We also evaluated contributions for higher resonances, but none of them had an effect as much as or larger than the case (d).

In summary, the resonances at 8.90 MeV and 9.20 MeV have a possibility to give significant contributions to the reaction rate for  $T_9 = 1.5$ – $3$ , although they are unlikely to be more than the contribution of the 8.420-MeV res-

onance, which dominates the reaction rate. Considering that the  $\Gamma_\gamma$  used here could be underestimated by factors and the decay widths and  $J^\pi$  are also uncertain, more studies are favored for the determination of resonant parameters in the energy region of  $E_{\text{ex}} = 8.5$ – $9.5$  MeV, which might be difficult to access from the  ${}^{10}\text{B}+p$  channel. On the other hand, the resonances above 9.5 MeV can be considered as negligible for  $T_9 < 10$ .

## VII. SUMMARY

We have studied resonant states for  $E_{\text{ex}} = 8.7$ – $13.0$  MeV in  ${}^{11}\text{C}$  via  $\alpha$ -resonant elastic scattering with the thick-target method in inverse kinematics, using a low-energy  ${}^7\text{Be}$  beam at CRIB.

We obtained excitation functions of  ${}^7\text{Be}(\alpha, \alpha_0){}^7\text{Be}$ ,  ${}^7\text{Be}(\alpha, \alpha_1){}^7\text{Be}^*$ ,  ${}^7\text{Be}(\alpha, p_0){}^{10}\text{B}$ , and  ${}^7\text{Be}(\alpha, p_1){}^{10}\text{B}^*$  simultaneously, measuring  $\gamma$ -rays in coincidence with  $\alpha$  particle or  $p$ . The excitation function of the elastic scattering exhibited strong  $\alpha$  resonances mostly in agreement with previous measurements, and we brought new information on the resonance parameters with an R-matrix analysis. The  ${}^7\text{Be}(\alpha, p_0){}^{10}\text{B}$  excitation function was consistent with the previous measurement of the inverse reaction,  ${}^{10}\text{B}(p, \alpha){}^7\text{Be}$ . The excitation functions were compared with the ones by a similar measurement performed recently [26], and we found differences in the absolute cross section and the energy, although their spectral shapes had a similarity.

A new negative parity band, which could have  $2\alpha$ - ${}^3\text{He}$  cluster structure, is proposed in  ${}^{11}\text{C}$ , in accordance with the previously proposed band in the mirror nucleus  ${}^{11}\text{B}$ . The resonant contribution for the astrophysical reaction rate of  ${}^7\text{Be}(\alpha, \gamma){}^{11}\text{C}$  was evaluated at high temperature using the new resonance parameters, and a 10%-order enhancement over the evaluation by NACRE could be expected for  $T_9 = 1.5$ – $3$ .

## ACKNOWLEDGMENTS

The experiment was performed at RI Beam Factory operated by RIKEN Nishina Center and CNS, the University of Tokyo. We are grateful to the RIKEN and CNS accelerator staff for their help. We truly appreciate Prof. Y.K. En'yo and Mr. T. Suhara for useful discussions and suggestions based on their theoretical calculations. This work was partly supported by JSPS KAKENHI (No. 21340053) and the Grant-in-Aid for the Global COE Program “The Next Generation of Physics, Spun from Universality and Emergence” from the Ministry of Education, Culture, Sports, Science and Technology (MEXT) of Japan. One of us (L.H. Khiem) wishes to acknowledge the support by Vietnam National Foundation for Science and Technology (NAFOSTED) under Contract No.103.04.54.09.

TABLE II. Parameters used in the reaction rate calculation. The dominant destination states of the  $\gamma$  decay according to our calculation are also shown.

	$E_{\text{ex}}$	$J^\pi$	$\Gamma_{\text{tot}}$ (keV)	$\Gamma_\alpha$ (keV)	$\Gamma_\gamma$ (eV)	$\omega$	$\omega\gamma$ (eV)	dominant dest.
(a)	8.90	$9/2^+$	8	8	0.48	2.5	1.2	8.655 MeV ( $7/2^+$ )
(b)	8.90	$3/2^+$	8	8	1.7	1.0	1.7	ground ( $3/2^-$ )
(c)	9.20	$5/2^+$	500	13	34	1.5	1.3	ground ( $3/2^-$ )
(d)	9.97	$7/2^-$	218	153	0.97	2.0	1.4	6.90 MeV ( $5/2^+$ )

- [1] M. Wiescher, J. Görres, S. Graff, L. Buchmann, and F.-K. Thielemann, *Astrophys. J.* **343**, 352 (1989).
- [2] G. M. Fuller, S. E. Woosley, and T. A. Weaver, *Astrophys. J.* **307**, 675 (1986).
- [3] M. Hernanz, J. José, A. Coc, and J. Isern, *Astrophys. J.* **465**, L27 (1996).
- [4] D. Thomas, D. N. Schramm, K. A. Olive, G. J. Mathews, B. S. Meyer, and B. D. Fields, *Astrophys. J.* **430**, 291 (1994).
- [5] A. Coc, S. Goriely, Y. Xu, M. Saimpert, and E. Vangioni, *Astrophys. J.* **744**, 158 (2012).
- [6] S. Wanajo, H.-T. Janka, and S. Kubono, *Astrophys. J.* **729**, 46 (2011).
- [7] C. Fröhlich, P. Hauser, M. Liebendörfer, G. Martínez-Pinedo, F.-K. Thielemann, E. Bravo, N. Zinner, W. Hix, K. Langanke, A. Mezzacappa, et al., *Astrophys. J.* **637**, 415 (2006).
- [8] S. E. Hunt, R. A. Pope, and W. W. Evans, *Phys. Rev.* **106**, 1012 (1957).
- [9] A. B. Brown, C. W. Snyder, W. A. Fowler, and C. C. Lauritsen, *Phys. Rev.* **82**, 159 (1951).
- [10] G. B. Chadwick, T. K. Alexander, and J. B. Warren, *Can. Jour. Phys.* **34**, 381 (1956).
- [11] J. W. Cronin, *Phys. Rev.* **101**, 298 (1956).
- [12] J. Jenkin, L. Earwaker, and E. Titterton, *Nucl. Phys.* **50**, 516 (1964).
- [13] P. Paul, N. Puttaswamy, and D. Kohler, *Phys. Rev.* **164**, 1332 (1967).
- [14] H. Allan, M. Govindjee, and N. Sarma, *Proc. Phys. Soc.* **A69**, 350 (1956).
- [15] J. C. Overley and W. Whaling, *Phys. Rev.* **128**, 315 (1962).
- [16] J. W. Olness, E. K. Warburton, D. E. Alburger, and J. A. Becker, *Phys. Rev.* **139**, B512 (1965).
- [17] H. J. Hauser, M. Walz, F. Weng, G. Staudt, and P. K. Rath, *Nucl. Phys. A* **456**, 253 (1986).
- [18] G. Hardie, B. W. Filippone, A. J. Elwyn, M. Wiescher, and R. E. Segel, *Phys. Rev. C* **29**, 1199 (1984).
- [19] A. Tohsaki, H. Horiuchi, P. Schuck, and G. Röpke, *Phys. Rev. Lett.* **87**, 192501 (2001).
- [20] Y. Kanada-En'yo, *Phys. Rev. C* **75**, 024302 (2007).
- [21] T. Kawabata, H. Akimune, H. Fujimura, H. Fujita, Y. Fujita, M. Fujiwara, K. Hara, K. Y. Hara, K. Hatanaka, T. Ishikawa, et al., *Phys. Rev. C* **70**, 034318 (2004).
- [22] T. Kawabata, H. Akimune, H. Fujita, Y. Fujita, M. Fujiwara, K. Hara, K. Hatanaka, M. Itoh, Y. Kanada-En'yo, S. Kishi, et al., *Phys. Lett. B* **646**, 6 (2007).
- [23] I. Ragnarsson, S. Åberg, H.-B. Håkansson, and R. Sheline, *Nucl. Phys. A* **361**, 1 (1981).
- [24] N. Soić, M. Freer, L. Donadille, N. Clarke, P. Leask, W. Catford, K. Jones, D. Mahboub, B. Fulton, B. Greenhalgh, et al., *Nucl. Phys. A* **742**, 271 (2004).
- [25] H. Yamaguchi, T. Hashimoto, S. Hayakawa, D. N. Binh, D. Kahl, S. Kubono, Y. Wakabayashi, T. Kawabata, and T. Teranishi, *Phys. Rev. C* **83**, 034306 (2011).
- [26] M. Freer, N. L. Achouri, C. Angulo, N. I. Ashwood, D. W. Bardayan, S. Brown, W. N. Catford, K. A. Chipps, N. Curtis, P. Demaret, et al., *Phys. Rev. C* **85**, 014304 (2012).
- [27] S. Kubono, Y. Yanagisawa, T. Teranishi, S. Kato, T. Kishida, S. Michimasa, Y. Ohshiro, S. Shimoura, K. Ue, S. Watanabe, et al., *Eur. Phys. J.* **A13**, 217 (2002).
- [28] Y. Yanagisawa, S. Kubono, T. Teranishi, K. Ue, S. Michimasa, M. Notani, J. J. He, Y. Ohshiro, S. Shimoura, S. Watanabe, et al., *Nucl. Instrum. Meth. Phys. Res., Sect. A* **539**, 74 (2005).
- [29] K. P. Artemov, O. P. Belyanin, A. L. Vetoshkin, R. Wolski, M. S. Golovkov, V. Z. Gol'dberg, M. Madeja, V. V. Pankratov, I. N. Serikov, V. A. Timofeev, et al., *Sov. J. Nucl. Phys* **52**, 408 (1990).
- [30] H. Yamaguchi, Y. Wakabayashi, G. Amadio, S. Hayakawa, H. Fujikawa, S. Kubono, J. He, A. Kim, and D. Binh, *Nucl. Instrum. Meth. Phys. Res., Sect. A* **589**, 150 (2008).
- [31] H. Kumagai, A. Ozawa, N. Fukuda, K. Sümmerer, and I. Tanihata, *Nucl. Instrum. Meth. Phys. Res., Sect. A* **470**, 562 (2001).
- [32] A. Alexandrov, I. Alexandrova, S. Podshibyakin, Y. Pyatkov, A. Slyusarenko, A. Shemetov, V. Gayshan, V. Kogan, and V. Pikul, *Nucl. Instrum. Meth. Phys. Res., Sect. A* **312**, 542 (1992).
- [33] G. Poggi, M. Bini, P. DelCarmine, F. Meucci, A. Olmi, A. Stefanini, and N. Taccetti, *Nuclear Instruments and Methods in Physics Research Section B: Beam Interactions with Materials and Atoms* **119**, 375 (1996).
- [34] J. Ziegler, J. Biersack, and M. Ziegler, *SRIM The Stopping and Range of Ions in Matter* (Lulu Press, Morrisville, USA, 2008).
- [35] N. Larson, *A Code System for Multilevel R-Matrix Fits to Neutron Data Using Bayes' Equations*, ORNL/TM-9179/R5 (2000; unpublished).
- [36] F. Ajzenberg-Selove, *Nucl. Phys. A* **506**, 1 (1990).
- [37] M. Wiescher, R. N. Boyd, S. L. Blatt, L. J. Rybarczyk, J. A. Spizuoco, R. E. Azuma, E. T. H. Clifford, J. D. King, J. Görres, C. Rolfs, et al., *Phys. Rev. C* **28**, 1431 (1983).
- [38] D. Tilley, J. Kelley, J. Godwin, D. J. Millener, J. E. Purcell, C. G. Sheu, and H. R. Weller, *Nucl. Phys. A*

- 745**, 155 (2004).
- [39] R. B. Day and T. Huus, Phys. Rev. **95**, 1003 (1954).
  - [40] G. R. Smith, J. R. Shepard, R. L. Boudrie, R. J. Peterson, G. S. Adams, T. S. Bauer, G. J. Igo, G. Pauletta, C. A. Whitten, A. Wriekat, et al., Phys. Rev. C **30**, 593 (1984).
  - [41] B. A. Watson, C. C. Chang, and M. Hasinoff, Nucl. Phys. A **173**, 634 (1971).
  - [42] W. Benenson, E. Kashy, D. H. Kong-A-Siou, A. Moalem, and H. Nann, Phys. Rev. C **9**, 2130 (1974).
  - [43] H. Kuan, M. Hasinoff, W. O'Connell, and S. Hanna, Nuclear Physics A **151**, 129 (1970).
  - [44] N. Itagaki, H. Masui, M. Ito, and S. Aoyama, Phys. Rev. C **71**, 064307 (2005).
  - [45] N. Itagaki, H. Masui, and J. Cseh, Journal of Physics: Conference Series **111**, 012006 (2008).
  - [46] T. Suhara and Y. Kanada-En'yo, Phys. Rev. C **85**, 054320 (2012).
  - [47] C. Angulo *et al.*, Nucl. Phys. A **656**, 3 (1999).
  - [48] Y. Xu, K. Takahashi, S. Goriely, and M. Arnould, AIP Conf. Proc. **1377**, 463 (2011).